ADVANCED FUNCTIONAL MATERIALS
www.afm-journal.de

Materials Views
www.MaterialsViews.com

Shape- and Size-Controlled Synthesis of Uniform Anatase TiO_2 Nanocuboids Enclosed by Active {100} and {001} Facets

*Xiaowei Zhao, Wenzui Jin, Jinguang Cai, Jianfeng Ye, Zhenhu Li, Yurong Ma, Jinglin Xie, and Limin Qi**

Uniform anatase TiO_2 nanocuboids enclosed by active {100} and {001} facets over a wide size range (60–830 nm in length) with controllable aspect ratios were solvothermally synthesized through hydrolysis of titanium tetraisopropoxide (TTIP) using acetic acid (HAc) as the solvent and the ionic liquid 1-butyl-3-methylimidazolium tetrafluoroborate ([bmim][BF_4]) as the capping agent. The size and aspect ratio of the anatase TiO_2 nanocuboids can be readily adjusted by changing the composition parameters including the contents of [bmim][BF_4], water, and HAc in the quaternary solution system. It was revealed that [bmim][BF_4] played an important role in stabilizing both the {100} and {001} facets of the anatase TiO_2 nanocuboids. On the one hand, [bmim][BF_4] acted as a fluoride source to release F^- ions for stabilizing the {001} facets; on the other hand, the $[bmim]^+$ ions acted as effective capping ions to preferentially stabilize the {100} facets. The obtained near-monodisperse anatase TiO_2 nanocuboids exhibited an interesting self-assembly behavior during deposition. These single-crystalline anatase nanocuboids showed extremely high crystalline phase stability, retaining the pure phase of anatase as well as the morphology even after being calcined at 900 °C. Moreover, the anatase nanocuboids exhibited considerably enhanced photocatalytic activity owing the wholly exposed active {100} and {001} facets.

1. Introduction

Recently, the shape-controlled synthesis of micro- and nanocrystals with exposed high-energy or active facets has attracted intensive interest because they usually exhibit fascinating surface-dependent properties and may find promising applications in a variety of technologically important areas including catalysis, sensing, or energy storage and conversion.[1–4] Anatase titanium dioxide (TiO_2), with a tetragonal crystal structure, is one of the most important semiconductors and has been widely used in photocatalysis, solar cells, photochromic devices, lithium-ion batteries, gas sensors, surface coatings, etc.[5,6] Theoretical calculations indicate that the {101} surface facets are the thermodynamically most stable facets for anatase TiO_2, while the {001} facets and {100} facets are active facets with a high surface energy.[7,8] Specifically, it has been documented that the order of the average surface energies of anatase TiO_2 is 0.90 J m^{-2} for {001} >0.53 J m^{-2} for {100} >0.44 J m^{-2} for {101}.[7] According to the Wulff construction, the equilibrium shape of an anatase crystal is a slightly truncated tetragonal bipyramid enclosed by eight {101} facets and two {001} facets, with the most stable {101} facets accounting for 94% of the total surface (**Scheme 1**a).[9] Since the {101} facets are quite unreactive, leading to limited activity for anatase crystals with the conventional shape, it is appealing to synthesize well-defined anatase TiO_2 crystals with a large percentage of exposed high-energy {001} or {100} facets.[10]

Since the pioneering work by Lu and co-workers on the synthesis of micrometer-sized anatase crystals with a large percentage of {001} facets by using fluorine to stabilize the active {001} facets,[3] there has been remarkable interest in the controlled synthesis of anatase crystals with varied percentages of exposed {001} facets, such as truncated tetragonal bipyramids (Scheme 1b) and square sheets (Scheme 1c).[11–13] Meanwhile, considerable efforts have been devoted to the synthesis and applications of hierarchical structures consisting of anatase nanocrystals with exposed {001} facets.[6,14] Compared with the significant progress made on the anatase crystals with dominant {001} facets, there has been only limited success achieved on the preparation of anatase crystals with a large percentage of {100} facets.[10,15–18] In particular, tetragonal nanorods of anatase crystals with a large percentage of lateral {100} facets, which showed four elongated {100} facets and two acute ends, were synthesized by hydrothermal transformation of alkali titanate nanotubes in basic solution.[17] It is noteworthy that micrometer-sized, elongated truncated tetragonal bipyramids of

X. Zhao, W. Jin, J. Cai, J. Ye, Z. Li, Dr. Y. Ma, Prof. J. Xie, Prof. L. Qi
Beijing National Laboratory for Molecular Sciences (BNLMS)
State Key Laboratory for Structural Chemistry of Unstable and Stable Species
College of Chemistry
Peking University
Beijing 100871, P. R. China
E-mail: liminqi@pku.edu.cn

DOI: 10.1002/adfm.201100629

© 2011 WILEY-VCH Verlag GmbH & Co. KGaA, Weinheim

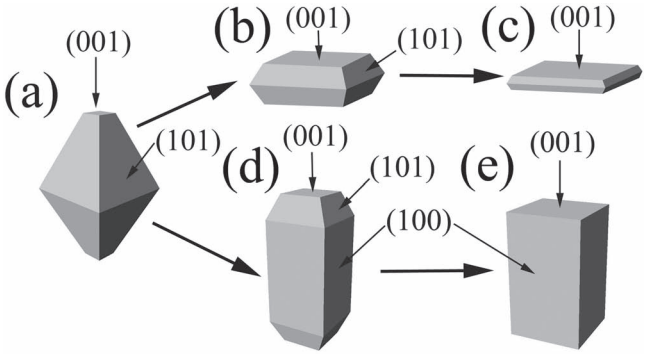

Scheme 1. Schematic drawings of anatase shapes: a) slightly truncated tetragonal bipyramid with dominant {101} facets (equilibrium crystal shape); b) truncated tetragonal bipyramid with a large percentage of top {001} facets; c) square sheet with dominant {001} facets; d) elongated truncated tetragonal bipyramid with a large percentage of lateral {100} facets; e) tetragonal cuboid enclosed by {100} and {001} facets.

anatase crystals with a large percentage of lateral {100} facets (Scheme 1d), which were enclosed by {100}, {101}, and {001} facets with percentages around 53%, 33%, and 14%, respectively, were synthesized by hydrothermal reaction in aqueous HF solution.[18] However, it remains a challenge to prepare well-defined, tetragonal cuboids of anatase crystals exclusively enclosed by {100} and {001} facets (Scheme 1e), although micrometer-sized, anatase nanosheets fully exposed with {001} (98.7%) and {100} (1.3%) facets were recently produced through a solvothermal route in 1-butanol solvent containing HF.[19] Untill now, there has been a controversy on the relative reactivity between the {001} and {100} facets of anatase crystals.[18] The preparation of uniform anatase cuboids enclosed by {100} and {001} facets with varied percentages would be helpful for evaluating the order of facet reactivity for different photocatalytic reactions. Moreover, the size and exposed facets of anatase crystals greatly influence their optical and electrochemical properties, and hence their performance for applications including solar cells and lithium-ion batteries.[6b,c,13c,d] Therefore, it is highly desirable to achieve the shape (or aspect ratio)-controlled synthesis of uniform anatase cuboids exclusively enclosed by {100} and {001} facets over a wide size range.

It may be noted that most of the reported anatase nanocrystals with active {001} and {100} facets, such as the elongated truncated bipyramids enclosed by {100}, {101}, and {001} facets[18] and the square nanosheets wholly exposed with {001} and {100} facets,[19] were produced in the presence of extremely corrosive and toxic hydrofluoric acid. Recently, ionic liquids have shown great potential in the shape-controlled synthesis of inorganic nanocrystals as environmentally benign solvents.[20,21] Particularly, truncated tetragonal bipyramids[22] and square sheets[13a] of anatase crystals with a large percentage of reactive {001} facets were synthesized in the ionic liquid 1-butyl-3-methylimidazolium tetrafluoroborate ([bmim][BF_4]) without using HF. Recently, we demonstrated that acetic acid (HAc) can be used as an effective solvent for the controlled synthesis of unique nanoporous anatase TiO_2 mesocrystals with a single-crystal-like structure, where HAc played multiple key roles during the sol–gel process of the titanium alkoxide precursor.[23] Herein, we report a novel solvothermal synthesis of uniform anatase TiO_2 nanocuboids enclosed by active {100} and {001} facets over a wide size range (60–830 nm in length) with controllable aspect ratios using HAc as the solvent and [bmim][BF_4] as the capping agent. The obtained near-monodisperse anatase TiO_2 nanocuboids exhibited interesting self-assembly behavior during deposition. Moreover, they showed remarkable crystalline-phase stability due to their single-crystalline nature, and considerably enhanced photocatalytic activity toward the formation of active hydroxyl radicals owing to the wholly exposed active {100} and {001} facets.

2. Results and Discussion

2.1. Synthesis of Anatase TiO_2 Nanocuboids

Anatase TiO_2 nanocuboids with varied sizes and aspect ratios were solvothermally synthesized in a quaternary solution system consisting of titanium tetraisopropoxide (TTIP), water, [bmim][BF_4], and HAc, with molar ratios of TTIP/H_2O/[bmim][BF_4]/HAc at 1:*x*:*y*:*z*, where the contents of water (*x*), [bmim][BF_4] (*y*), and HAc (*z*) were systematically changed. In a typical synthesis, 200 μL of TTIP, 200 μL of [bmim][BF_4], 20 μL of water, and 8 mL of HAc were mixed to give a reaction solution with molar ratios of TTIP/H_2O/[bmim][BF_4]/HAc at 1:1.66:2:210. **Figure 1**a shows an overview given by a scanning electron microscopy (SEM)

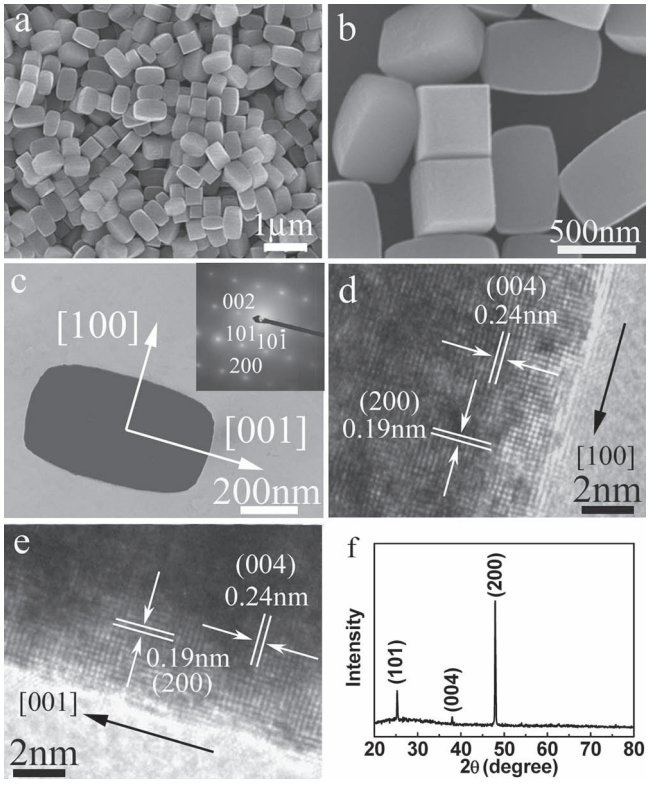

Figure 1. SEM (a,b), TEM (c), and HRTEM (d,e) images and XRD pattern (f) of anatase TiO_2 nanocuboids obtained from the TTIP/H_2O/[bmim][BF_4]/HAc system with molar ratios at 1:1.66:2:210. The nset shows the related SAED pattern.

© 2011 WILEY-VCH Verlag GmbH & Co. KGaA, Weinheim

image of the product, which suggests the large-scale formation of uniform nanocuboids with a length of 660 ± 50 nm and an edge width of 370 ± 30 nm. A magnified image is presented in Figure 1b, which clearly shows that the tetragonal nanocuboids with sharp edges have barlike lateral facets and squarelike top facets. Figure 1c shows the transmission electron microscopy (TEM) image of a single nanocuboid lying on its one lateral facet together with the corresponding selected-area electron diffraction (SAED) pattern, which exhibits sharp diffraction spots ascribed to the [010] zone axis of the tetragonal anatase TiO_2 crystal, indicating that the nanocuboid is a [001]-elongated anatase single crystal with four {100} lateral facets and two {001} top facets. This result is confirmed by high-resolution TEM (HRTEM) images taken from the edges of a top facet (Figure 1d) and a lateral facet (Figure 1e), which exhibit clear lattice fringes with d spacings of 0.19 nm and 0.24 nm that can be indexed to the (200) and (004) planes of tetragonal anatase, respectively. Figure 1f presents the powder X-ray diffraction (XRD) pattern of the obtained nanocuboids, which shows reflections characteristic of anatase TiO_2 with the tetragonal structure (JCPDS Card 21–1272), demonstrating the formation of pure anatase TiO_2 crystals. It is noteworthy that the intensity of the (200) reflection is significantly enhanced compared with its standard intensity, which can be rationalized by considering that the nanocuboids enclosed by larger lateral {100} facets and smaller top {001} facets tended to lie on their lateral {100} facets during deposition on the substrate surface for the XRD characterization.

These results suggest that uniform, well-defined, tetragonal nanocuboids of anatase TiO_2 almost entirely enclosed by active {100} and {001} facets were successfully synthesized in the TTIP/H_2O/[bmim][BF_4]/HAc system. Considering that anatase TiO_2 adopts a tetragonal structure with lattice parameters $a = b = 0.377$ nm and $c = 0.950$ nm, the formation of tetragonal nanocuboids of anatase TiO_2 with two top {001} facets and four lateral {100} facets would be favored due to the crystal symmetry once the {001} and {100} facets are stabilized by certain capping agents. It is thus speculated that the current TTIP/H_2O/[bmim][BF_4]/HAc system may be favorable for the selective stabilization of the {001} and {100} facets, and the size and aspect ratio of the nanocuboids may be adjusted by changing the composition parameters. Actually, it was found that the contents of water (x), [bmim][BF_4] (y) and HAc (z) played key roles in controlling the shape and size of the anatase TiO_2 crystals obtained in this quaternary system. Accordingly, a variety of anatase TiO_2 nanocuboids enclosed by {100} and {001} facets with different sizes, aspect ratios, and percentages of the {100} facets (S_{100}, estimated from the length (a) and width (b) of the nanocuboids by assuming a shape of perfect tetragonal cuboids) were produced through systematically changing the composition parameters, which is summarized in **Table 1**. Particularly, the percentage of the exposed (100) and (001) facets of the typical anatase TiO_2 nanocuboids shown in Figure 1 was estimated to be 78.2% and 21.8%, respectively.

Figure 2 shows the products obtained in the quaternary system with different [bmim][BF_4] contents (y) while the other composition parameters were kept unchanged. When the synthesis was conducted without [bmim][BF_4], only ellipsoidal particles about several hundred nanometers in size were obtained (Figure 2a), which adopted a pure anatase TiO_2 phase,

Table 1. Size parameters of anatase TiO_2 nanocuboids obtained from the quaternary TTIP/H_2O/[bmim][BF_4]/HAc system with varied molar ratios of 1:x:y:z. a and b represent the length and width of tetragonal nanocuboids, respectively. a/b represents the aspect ratio and S_{100} represents the percentage of the {100} facets, which is equal to $2a/(2a + b)$.

Molar ratio (1: x: y: z)	a [nm]	b [nm]	a/b	S_{100} [%]
1: 1.66: 1: 210	460	250	1.84	78.6
1: 1.66: 2: 210	660	370	1.78	78.2
1: 1.66: 5: 210	830	490	1.69	77.2
1: 4.15: 2: 210	510	290	1.76	77.9
1: 8.3: 2: 210	380	220	1.73	77.6
1: 16.6: 2: 210	255	150	1.7	77.3
1: 41.5: 2: 210	120	110	1.09	68.6
1: 1.66: 2: 105	560	290	1.93	79.4
1: 1.66: 2: 53	525	265	1.98	79.8
1: 1.66: 2: 26	460	190	2.42	82.9
1: 1.66: 2: 13	350	120	2.92	85.3
1: 1.66: 2: 5.3	60	20	3.0	85.7

as revealed by the corresponding XRD pattern (Figure S1, Supporting Information). When a small amount of [bmim][BF_4] ($y = 1$) was added to the solution, well-faceted anatase TiO_2 nanocuboids ≈460 nm in length and ≈250 nm in width were obtained (Figure 2b), which were somewhat smaller than the typical nanocuboids obtained at $y = 2$ (Figure 1). When the [bmim][BF_4] content was increased to $y = 5$, larger anatase TiO_2 nanocuboids ≈830 nm in length and ≈490 nm in width were obtained, indicating a continued increase in the cuboid size with increasing [bmim][BF_4] content. However, if the [bmim][BF_4] content was too large (e.g., $y = 10$), some anatase TiO_2 nanocuboids coexisted with a large amount of irregular aggregates, which adopted an unknown crystalline phase, as revealed by the corresponding XRD result (Figure S1, Supporting Information). This result suggests that the presence of

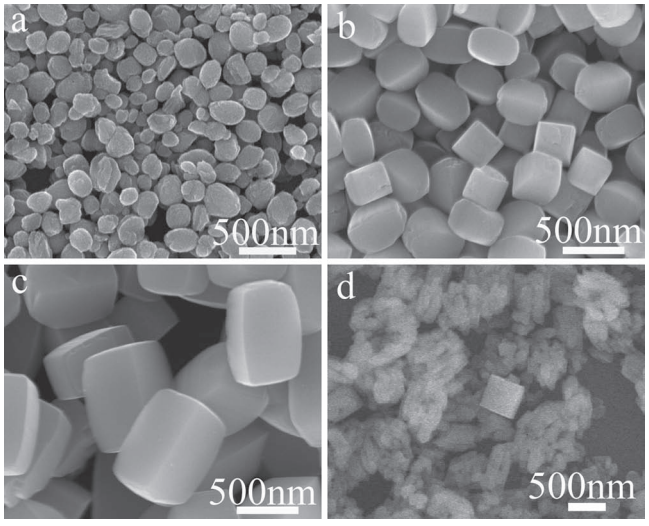

Figure 2. SEM images of products obtained in the TTIP/H_2O/[bmim][BF_4]/HAc system with molar ratios of 1:1.66: y: 210 at different [bmim][BF_4] contents (y): a) 0, b) 1, c) 5, d) 10.

© 2011 WILEY-VCH Verlag GmbH & Co. KGaA, Weinheim

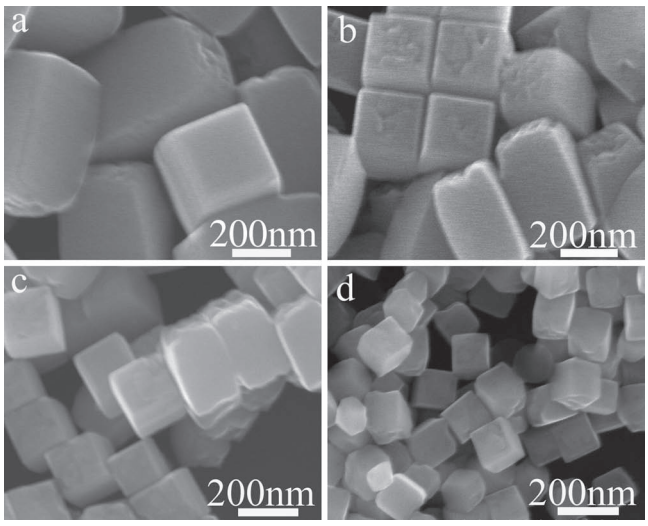

Figure 3. SEM images of anatase TiO_2 nanocuboids obtained in the TTIP/H_2O/[bmim][BF_4]/HAc system with molar ratios of 1: *x*: 2: 210 at different water contents (*x*): a) 4.15, b) 8.3, c) 16.6, d) 41.5.

a suitable content of [bmim][BF_4] was essential to the exclusive formation of the anatase TiO_2 nanocuboids. It is indicated that [bmim][BF_4] could play an important role in stabilizing both the {100} and {001} facets of anatase TiO_2 crystals.

For the sol-gel process of titanium alkoxide ($Ti(OR)_4$) in non-aqueous solution containing a very small amount of water, the water content would significantly influence the hydrolysis and condensation rate of $Ti(OR)_4$ and thus the formation of anatase nanocrystals.[10,24] For the synthesis in the current TTIP/H_2O/[bmim][BF_4]/HAc system, if no adscititious water was added to the reaction solution, only a mixture of a small amount of anatase nanocuboids and a large amount of irregular aggregates were obtained. When a minor amount of water ($x = 1.66$) was added, uniform anatase TiO_2 nanocuboids enclosed by {100} and {001} facets were obtained, as shown in Figure 1. When the water content was increased, a series of uniform anatase TiO_2 nanocuboids with varied sizes and aspect ratios were produced, as shown in **Figure 3**. Specifically, with increasing the water content (*x*) from 1.66 to 41.5, the length of the nanocuboids was gradually decreased from 660 nm to 120 nm and the aspect ratio was gradually decreased from 1.78 to 1.09. Since the increase in the water content would considerably accelerate the hydrolysis and condensation process as well as the nucleation and growth of anatase nanocrystals, a higher water content would lead to the rapid formation of a larger amount of anatase TiO_2 nuclei, resulting in the final anatase TiO_2 nanocuboids with a smaller size. However, if the water content was further increased to too large (e.g., $x > 83$), truncated bipyramids of anatase TiO_2 would appear in addition to the anatase TiO_2 nanocuboids, indicating that a too large water content would impair the role of [bmim][BF_4] in stabilizing the {100} and {001} facets of anatase crystals, favoring the appearance of {101} facets.

The SEM images of the obtained anatase TiO_2 nanocuboids shown in Figure 3 exhibit two additional features worth mentioning. First, the top {001} facets of the nanocuboids were mildly etched to exhibit a slightly rugged surface, while the lateral {100} facets were kept smooth. This phenomenon is reminiscent of the selective etching of the {001} facets of the anatase TiO_2 truncated bipyramids by HF.[25] Second, some nanocuboids were self-assembled side-by-side into regular two-dimensional (2D) aggregates (Figure 3b), indicating that the near-monodisperse anatase TiO_2 nanocuboids could potentially act as unique building blocks for constructing hierarchically ordered assemblies or colloidal crystals. It has been documented that the self-assembly of nanoparticles in solution can be driven by various interparticle forces, such as van der Waals forces, electrostatic forces, molecular surface forces, and entropic effects.[26a] In particular, translational and orientational excluded-volume fields encoded in particles with anisotropic shapes can lead to purely entropy-driven assembly of morphologies with specific order and symmetry.[26b] In the current situation, the side-by-side self-assembly of the nanocuboids without surface functionalization could be ascribed to an entropy-driven process, which has been frequently used to explain the side-by-side assembly of hard rods in solution.[26a] Moreover, the side-by-side assembly would be more stable than the end-to-end assembly for the tetragonal nanocuboids with four smooth lateral faces and two slightly rugged top faces since the side-by-side assembly tends to form a close-packed geometry with maximized interparticle van der Waals interactions.[26c]

It is known that chemical modification of $Ti(OR)_4$ by carboxylic acids is a rational strategy to tune the reactivity of the precursor toward water;[24] particularly, HAc can adjust the reactivity of TTIP through the coordination with titanium centers, thereby influencing the nucleation and growth of anatase TiO_2 nanocrystals. As shown in **Figure 4**, a series of uniform

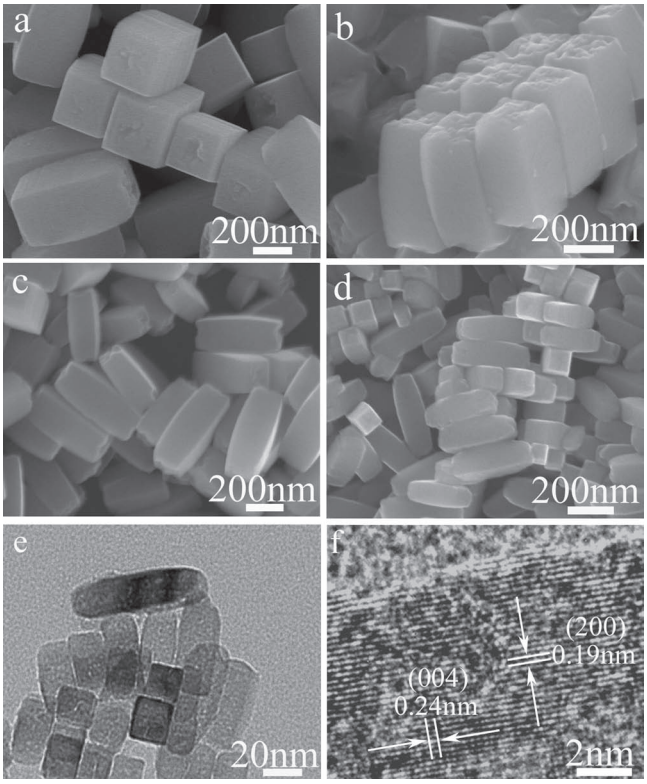

Figure 4. SEM (a–d), TEM (e) and HRTEM (f) images of anatase TiO_2 nanocuboids obtained in the TTIP/H_2O/[bmim][BF_4]/HAc system with molar ratios of 1:1.66:2:*z* at different HAc contents (*z*): a) 105, b) 53, c) 26, d) 13, e,f) 5.3.

© 2011 WILEY-VCH Verlag GmbH & Co. KGaA, Weinheim

anatase TiO_2 nanocuboids with varied sizes and aspect ratios were produced when the HAc content (*z*) was decreased. Specifically, with decreasing the HAc content (*z*) from 210 to 13, the length of the nanocuboids was gradually decreased from 660 nm to 310 nm and the aspect ratio was gradually increased from 1.78 to 2.92 (Figure 4a–d). When the HAc content was further decreased to 5.3, the length of the nanocuboids was significantly decreased to 60 nm and the aspect ratio was further increased 3.0 (Figure 4e). The related HRTEM image confirmed that the nanocuboid was a [001]-elongated single crystal with four lateral {100} facets (Figure 4f). Since the decrease in the HAc content would considerably weaken the hindering of the hydrolysis-condensation process, a low HAc content would lead to the rapid formation of a larger amount of anatase TiO_2 nuclei, resulting in the final anatase TiO_2 nanocuboids with a smaller size, similar to the case of increase in the water content. However, the variation trend in the aspect ratio with decreasing HAc content was different from that with increasing water content. In other word, the increase in both the water content (*x*) and the HAc content (*z*) resulted in the decrease in the aspect ratio or the percentage of the {100} facets. It is worth mentioning that the side-by-side self-assembly of the uniform nanocuboids into regular 2D aggregates was evident (Figure 4b), further indicating their potential applications as unique building blocks for constructing hierarchically ordered assemblies or colloidal crystals with novel properties.

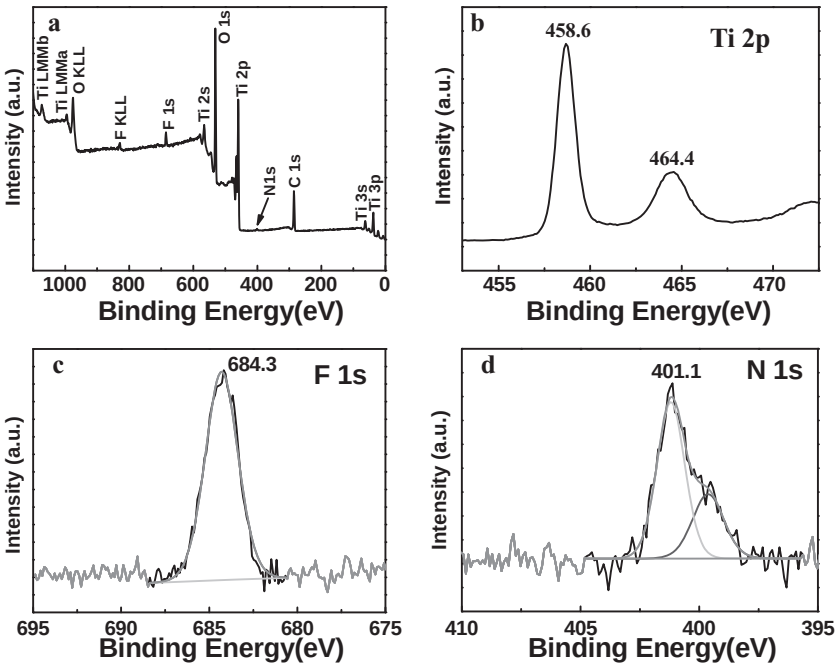

Figure 5. X-ray photoelectron survey spectrum (a) and fine scans of Ti1s (b), F1s (c), and N1s (d) of anatase TiO_2 nanocuboids obtained from the TTIP/H_2O/[bmim][BF_4]/HAc system with molar ratios at 1:1.66:2:210.

2.2. Formation Mechanism of Anatase TiO_2 Nanocuboids

The investigation on the effects of the composition parameters suggests that besides the solvent HAc and the reagent water, the additive [bmim][BF_4] played a key role in the formation of the anatase TiO_2 nanocuboids enclosed by {100} and {001} facets. To shed light on the interaction of [bmim][BF_4] with the anatase nanocuboids, X-ray photoelectron (XPS) spectra of the as-prepared anatase TiO_2 nanocuboids were measured, which were shown in **Figure 5**. XPS peaks characteristic of Ti, O, F, N, and C can be observed from the XPS survey spectrum (Figure 5a). The binding energies of Ti 2p3/2 and Ti 2p1/2 are 458.8 and 464.3 eV, respectively (Figure 5b), indicating that the oxidation state of the Ti element is the same as that of bulk TiO_2.[27] The binding energy of F 1s is 684.5 eV (Figure 5c), which is a typical value from F^- for fluorated TiO_2 system such as Ti–F species,[3] indicating the presence of the F^- ion instead of the $[BF_4]^-$ ion on the crystal surface. As shown in Figure 5d, the binding energy of N 1s is 401.1 eV, which can be attributed to the $[bmim]^+$ ion adsorbed on the surface of TiO_2 nanocrystals.[28] The presence of trace $[bmim]^+$ species on the nanocuboid surface was confirmed by the FTIR spectrum of the as-prepared anatase nanocuboids,[22,29] which showed weak absorption bands at 1452, 1168, and 1430 cm^{-1}, similar to the bands characteristic of $[bmim]^+$ ions from pure [bmim][Cl] (Figure S2, Supporting Information). These results suggest that the preferential adsorption of the F^- ions and $[bmim]^+$ ions on the specific surfaces of anatase crystals could largely contribute to the stabilization of the {100} and {001} facets.

It has been documented that $[BF_4]^-$ is inclined to decompose into F^- and other species under moisture conditions, thus providing a fluoride source;[30] Moreover, ionic liquids acting as a fluoride source are environmentally friendly and operationally safe compared with other erosive fluoride sources (such as HF).[31] In the current synthesis of the anatase TiO_2 nanocuboids enclosed by {100} and {001} facets, the ionic liquid [bmim][BF_4] could also act as a relatively mild fluoride source to release the necessary F^- ions for stabilizing specific facets of anatase crystals.

For elucidating the exact role played by [bmim][BF_4] in the synthesis of the anatase TiO_2 nanocuboids, a series of experiments were carried out to examine the effects of the $[bmim]^+$ ions, $[BF_4]^-$ ions, and F^- ions on the stabilization of the {100} and {001} facets of anatase crystals. **Figure 6** shows the result obtained by replacing [bmim][BF_4] with [bmim]Cl or Na[BF_4] under otherwise identical conditions. When [bmim]Cl was added instead of [bmim][BF_4], only ellipsoidal anatase particles were produced (Figure 6a), which is similar to the product obtained in the absence of [bmim][BF_4] (Figure 2a). When Na[BF_4] was added instead of [bmim][BF_4], well-defined, truncated tetragonal bipyramids or square sheets of anatase TiO_2 enclosed by a large percentage of top {001} facets and a minor percentage of lateral {101} facets were obtained as the exclusive

© 2011 WILEY-VCH Verlag GmbH & Co. KGaA, Weinheim

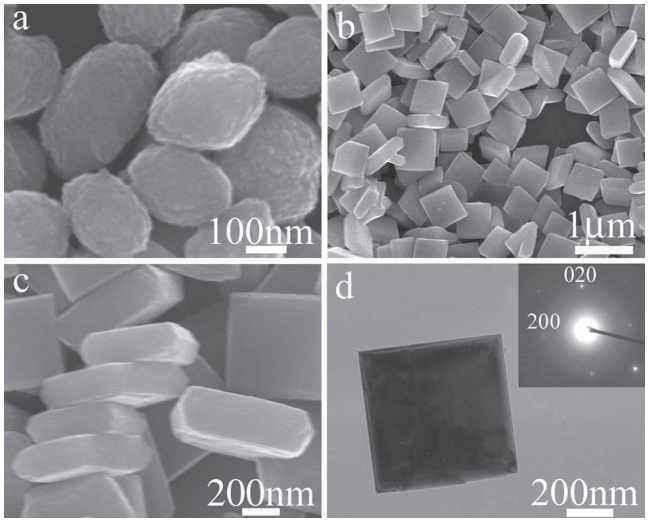

Figure 6. SEM (a–c) and TEM (d) images of anatase TiO_2 crystals obtained in the TTIP/H_2O/[bmim]Cl/HAc (a) and TTIP/H_2O/Na[BF_4]/HAc (b–d) systems with molar ratios of 1:1.66:2:210. The inset shows the related SAED pattern.

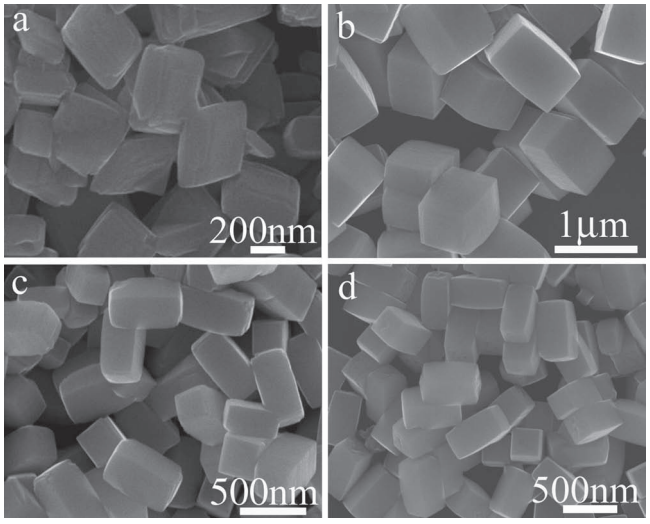

Figure 7. SEM images of anatase TiO_2 crystals obtained in the quinary TTIP/H_2O/[bmim]Cl/HF/HAc system with molar ratios of 1:1.66:*w*:0.82:210 at different [bmim]Cl contents (*w*): a) 0, b) 1, c) 2, d) 4.

product (Figure 6b–d). This result is not surprising since $[BF_4]^-$ ions are prone to hydrolyze and release F^- ions under the existence of hydration water, and the F^- ions are able to stabilize the {001} facets of anatase TiO_2 crystals. However, it is interesting to note that the presence of sole $[BF_4]^-$ ions or $[bmim]^+$ ions did not bring about the formation of anatase nanocuboids enclosed by {100} and {001} facets, indicating that there could be a cooperative effect of $[BF_4]^-$ ions and $[bmim]^+$ ions in the formation of the anatase nanocuboids with wholly exposed {100} and {001} facets.

Considering that the $[BF_4]^-$ ions mainly acted as the fluoride source to release the F^- ions, it is speculated that the ionic liquid [bmim][BF_4] could be replaced by a simple mixture of $[bmim]^+$ ions and F^- ions. This hypothesis was testified by the synthesis performed in a quinary TTIP/H_2O/[bmim]Cl/HF/HAc system with varied [bmim]Cl contents (*w*) and a fixed F^- ion content (about 0.4 times the typical $[BF_4]^-$ ion content), as shown in **Figure 7**. In the absence of [bmim]Cl, truncated tetragonal bipyramids of anatase TiO_2 dominated by the top {001} facets were obtained (Figure 7a). When a small amount of [bmim]Cl was added (*w* = 1), uniform, well-defined, anatase TiO_2 nanocuboids (≈900 nm in length and ≈640 nm in width) exclusively enclosed by {100} and {001} facets were produced (Figure 7b). When the [bmim]Cl content was gradually increased, uniform anatase nanocuboids with smaller sizes and higher aspect ratios were obtained (Figure 7c,d), which is summarized in **Table 2**. It is indicated that the percentage of the {100} facets was gradually increased with increasing [bmim]Cl content. This result demonstrated that the $[bmim]^+$ ions played an essential role in stabilizing the {100} facets of anatase crystals, thus favoring the formation of the final anatase TiO_2 nanocuboids with a large percentage of active {100} facets.

The role played by the $[bmim]^+$ ions in stabilizing the {100} facets of anatase crystals was confirmed by the synthesis performed in another quinary TTIP/H_2O/[bmim]Cl/[bmim][BF_4]/HAc system with varied [bmim]Cl contents (*w*) and a fixed [bmim][BF_4] content (Figure S3, Supporting Information). When [bmim]Cl was added to the typical quaternary TTIP/H_2O/[bmim][BF_4]/HAc system, uniform anatase TiO_2 nanocuboids with smaller sizes and higher aspect ratios were obtained (Table 2). It means that the percentage of the {100} facets was gradually increased with increasing [bmim]Cl content, confirming that the $[bmim]^+$ ions are able to stabilize the {100} facets of anatase TiO_2 crystals under the assistance of the F^- ions.

It has been shown that the F^- ions are very effective in stabilizing the {001} facets of anatase TiO_2 crystals because the surface-adsorbed fluorine atoms are able to considerably lower the surface energy of the {001} facets.[3] The current results showed that the addition of $[bmim]^+$ ions to the synthesis system containing $[BF_4]^-$ or F^- ions led to the appearance of the {100} facets accompanied by the disappearance of the {101} facets, resulting in a remarkable transition from truncated tetragonal bipyramids

Table 2. Size parameters of anatase TiO_2 nanocuboids obtained from the quinary TTIP/H_2O/[bmim]Cl/HF/HAc and TTIP/H_2O/[bmim]Cl/[bmim][BF_4]/HAc systems with molar ratios of 1:*x*:*w*:*y*:*z* at varied [bmim]Cl contents (*w*). *a* and *b* represent the length and width of tetragonal nanocuboids, respectively. *a*/*b* represents the aspect ratio and S_{100} represents the percentage of the {100} facets, which is equal to $2a/(2a + b)$.

Molar ratio (1: *x*: *w*: *y*: *z*)	*a* [nm]	*b* [nm]	*a*/*b*	S_{100} [%]
TTIP/H_2O/[bmim]Cl/HF/HAc				
1: 1.66: 1: 0.82: 210	900	640	1.41	73.8
1: 1.66: 2: 0.82: 210	540	300	1.80	78.3
1: 1.66: 4: 0.82: 210	500	250	2.00	80.0
TTIP/H_2O/[bmim]Cl/[bmim][BF_4]/HAc				
1: 1.66: 0.2: 2: 210	630	330	1.91	79.2
1: 1.66: 2: 2: 210	520	240	2.17	81.2
1: 1.66: 4: 2: 210	420	180	2.33	82.4

© 2011 WILEY-VCH Verlag GmbH & Co. KGaA, Weinheim

enclosed by {001} facets and {101} facets to tetragonal cuboids enclosed by {001} facets and {100} facets. This result strongly indicated that the $[bmim]^+$ ions could be preferentially adsorbed on the {100} facets of anatase crystals rather than the {101} facets. It has been documented that $[bmim]^+$ ions have preference for adsorbing on the TiO_2 crystal surface.[22,28] Generally, when the 1-alkyl-3-methylimidazolium cations are adsorbed on the TiO_2 surface, there may exist the electrostatic interaction, the van der Waals interaction, the hydrogen-bonding interaction existing in the O(TiO_2 surface)-H-C(imidazolium rings), as well as the mutual π-stacking interaction between aromatic rings.[32] The preferential adsorption of the $[bmim]^+$ ions on the {100} facets could be rationalized by comparing the surface structures of the (101) and (100) planes of anatase TiO_2 (Figure S4, Supporting Information).[32] The anatase (101) plane is toothed, and typical distances between bridging O atoms are 0.757 nm and 0.546 nm, which are not in the space range of the mutual π-stacking between aromatic rings (0.6–0.7 nm).[32] Therefore, it is impossible for the $[bmim]^+$ ions to perpendicularly adsorb on the (101) plane and construct a tight coverage layer. In contrast, the anatase (100) plane is relatively flat, and besides the distance of 0.757 nm along the [010] direction, typical distances between bridging O atoms within one (100) plane are 0.651 nm and 0.661 nm, which are in the space range of the mutual π-stacking between aromatic rings. Hence, the $[bmim]^+$ ions could be allowed to adsorb on the (100) plane to form a relatively tight coverage layer, which may account for the preferential adsorption of the $[bmim]^+$ ions on the {100} facets of anatase TiO_2.

Therefore, it may be concluded that F^- ions and $[bmim]^+$ ions contributed to the formation of the anatase TiO_2 nanocuboids enclosed by {100} and {001} facets in such a cooperative way: the strong binding interaction of the F^- ions to the {001} facets always led to the appearance of the stabilized top {001} facets together with less stable, lateral facets, and then the preferential adsorption of the $[bmim]^+$ ions to the {100} facets rather than the typical {101} facets resulted in the appearance of the stabilized {100} planes as the lateral facets. This mechanism could be used to tentatively explain the experimental phenomenon that the increase in both the water content (x) and the HAc content (z) resulted in the decrease in the aspect ratio of the anatase nanocuboids or the percentage of the {100} facets. An increase in the water content would greatly accelerate the hydrolysis-condensation process and thus weaken the stabilizing effect of the $[bmim]^+$ ions, leading to a decreased percentage of the {100} facets. On the other hand, an increase in the content of the HAc solvent means a dilution of the solution or a considerable decrease in the $[bmim]^+$ ion concentration, leading to a decreased percentage of the {100} facets.

In order to further illustrate the formation process of the anatase TiO_2 nanocuboids, a time-dependent investigation of the formation of the typical anatase TiO_2 nanocuboids shown in Figure 1 was carried out (Figure S5 and S6, Supporting Information). After 1 h of reaction, some micrometer-sized columnlike aggregates were formed together with irregular nanofiber networks showing a weak diffraction ring corresponding to a d spacing of ≈0.37 nm. The related XRD pattern suggests that while two broad diffraction peaks at d ≈0.37 nm and ≈0.19 nm may be attributed to the nanofiber networks, all the other diffractions peaks can be ascribed to the unknown phase previously identified for the irregular aggregates obtained at a high $[bmim][BF_4]$ content shown in Figure 2d (see Figure S1b, Supporting Information). This result indicates that anatase TiO_2 did not form at this early stage, and only the metastable columnlike aggregates with the unknown crystal phase (precursor I) and poorly crystallized nanofiber networks (precursor II) were produced. At a reaction time of 6 h, some anatase TiO_2 nanocuboids ≈300 nm in length appeared, in addition to the columnlike aggregates as well as the networks, which is consistent with the related XRD result. When the reaction time was increased to 12 h, all the columnlike aggregates disappeared and many anatase TiO_2 nanocuboids with a large size (≈400 nm in length) together with the crystalline nanofiber networks were produced, in good agreement with the related XRD pattern. If the reaction time were further increased to 24 h, uniform anatase TiO_2 nanocuboids ≈660 nm in length were obtained exclusively, as shown in Figure 1. These results suggest that in the current TTIP/H_2O/$[bmim][BF_4]$/HAc system, two types of metastable solid precursors quickly formed through the hydrolysis-condensation of TTIP in the presence of HAc and $[bmim][BF_4]$, prior to the formation of anatase TiO_2 crystals. Then, small anatase TiO_2 nanocuboids formed, which gradually grew up at the expense of the precursors and reached the final size when all the transient precursors were exhausted. Here, the metastable precursors acted as a reservoir to gradually release soluble titanium-containing species for the growth of the anatase TiO_2 nanocuboids, which is reminiscent of the formation of anatase TiO_2 mesocrystals through transformation from metastable precursors in acetic acid.[23]

2.3. Crystalline Phase Stability and Photocatalytic Activity

The anatase-to-rutile phase transformation in TiO_2 has attracted significant attention since the phase structure of titania crystals largely determine their suitability for practical applications in high-temperature environments.[33–35] Pure bulk anatase is considered widely to begin to transform irreversibly to rutile in air at ≈600 °C.[33] For anatase particles precipitated from solution, the transformation usually occurs at a temperature range of 500–700 °C under normal conditions, and many attempts including doping and surface modification have been made to inhibit the phase transformation of anatase.[34] The crystalline phase stability of the typical anatase TiO_2 nanocuboids shown in Figure 1 was investigated by examining the XRD patterns of the nanocuboids calcined at different temperatures for 3 h, which are shown in **Figure 8**. It can be seen that the single-crystalline anatase nanocuboids showed extremely high crystalline phase stability, retaining the pure phase of anatase even after being calcined at 900 °C. This crystalline phase stability is considerably higher than that of the single-crystalline anatase TiO_2 microsheets (≈2 μm in side length) dominated by {001} facets, which were thermally stable up to 800 °C.[13a] Remarkably, the anatase TiO_2 nanocuboids maintained their morphology even after calcination at 900 °C (Figure S7, Supporting Information). This is in contrast to the case of the single-crystal-like nanoporous anatase mesocrystals solvothermally synthesized in HAc, which retained the pure anatase phase after being calcined

© 2011 WILEY-VCH Verlag GmbH & Co. KGaA, Weinheim

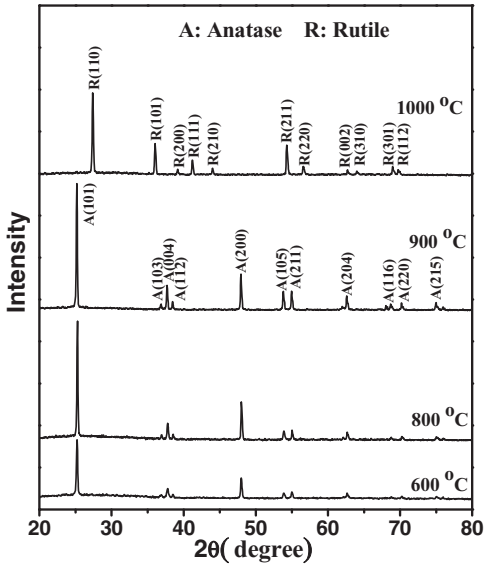

Figure 8. XRD patterns of anatase TiO_2 nanocuboids calcined at different temperatures.

at 900 °C but a sintering process occurred, resulting in a considerable change in the morphology.[23] Therefore, the current single-crystalline anatase nanocuboids with high-temperature stability in both crystalline phase and morphology may find promising applications in high-temperature environments, such as catalysis, gas sensors, and photoelectronic devices.

Since the anatase TiO_2 nanocuboids are almost exclusively enclosed by the active {100} and {001} facets, they may be expected to exhibit higher photoreactivity compared with normal anatase crystals. It has been demonstrated that the surface-adsorbed fluorine atoms can be easily removed to obtain fluorine-free, clean facets by simple calcination at temperatures above 600 °C.[3,18] Therefore, taking the typical anatase TiO_2 nanocuboids shown in Figure 1 as an example, the photocatalytic activity of the as-prepared anatase nanocuboids capped by F atoms (denoted as F-cuboids) and the fluorine-free, clean anatase nanocuboids obtained after calcination at 800 °C (denoted as clean cuboids) were measured using the anatase TiO_2 sheets shown in Figure 6b–d (calcined and denoted as clean sheets) and commercial Degussa P25 TiO_2 as the control samples. The photoreactivity was monitored by measuring the formation of active hydroxyl radicals (•OH) upon irradiation,[12a,17,18] which are considered as the most important oxidative species in photocatalysis reactions.[36] Terephthalic acid (TA) was used as a fluorescence probe, which emits a unique fluorescence signal with the emission peak around 426 nm, originated from 2-hydroxyterephthalic (TAOH) acid produced by the reaction of TA with •OH in basic solution. **Figure 9**a displays the fluorescence spectra of the UV light irradiated clean anatase nanocuboids in 3 mM terephthalic acid and 0.01 M NaOH solution at different irradiation times. The linear relationships between fluorescence intensity and irradiation time confirm the stability of anatase TiO_2 nanocuboids. The capability of forming •OH per unit surface area of clean nanocuboids, fluorine-capped nanocuboids, and P25, as for the basis for the comparison, was examined following the literature.[12a,17] Based on the Brunauer–Emmett–Teller (BET) surface area of the clean cuboids, F-cuboids, clean sheets and P25, which are 5.8, 5.0, 6.1, and 53.8 $m^2\ g^{-1}$, respectively, the normalized concentration of •OH generated from the three different photocatalysts are shown in Figure 9b. The normalized concentration of •OH generated from clean cuboids is ≈4.5 times as high as that of F-cuboids, indicating an enhanced photocatalytic activity after the fluorine removal as expected. The normalized photoreactivity of clean cuboids is ≈2.5 times as high as that of P25, which demonstrates substantially enhanced photoreactivity of the anatase TiO_2 nanocuboids bound by active {100} and {001} facets. Moreover, the normalized photoreactivity of clean cuboids is ≈3 times as high as that of clean sheets with a comparable surface area. This result suggests that the anatase TiO_2 cuboids with predominant {100} facets exhibited a considerably higher photocatalytic activity than the anatase TiO_2 sheets with predominant {001} facets, which is consistent with the recently reported higher photoreactivity of the {100} facets compared with the {001} facets.[18] These preliminary results indicate that the obtained anatase TiO_2 nanocuboids are promising photocatalyts; however, detailed investigation on the photoreactivity of anatase TiO_2 nanocuboids with systematically varied aspect ratios (or the relative proportion between the {100} and {001} facets) and sizes is needed to give a full evaluation of the order of facet reactivity for different photocatalytic reactions, which is currently under way.

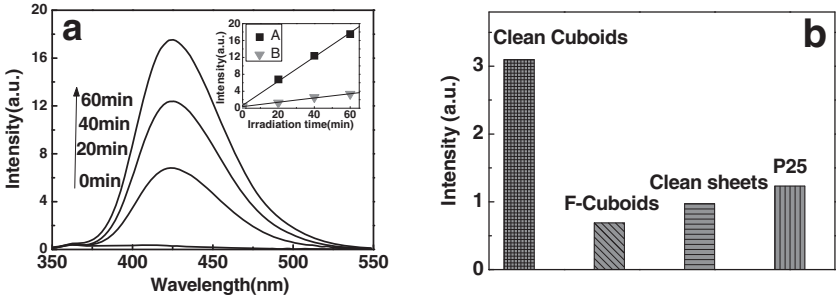

Figure 9. a) Fluorescence spectra of UV light (λ_{max} ≈ 254 nm) irradiation of anatase TiO_2 nanocuboids with fluorine-free surfaces in 3 mM terephthalic acid and 0.01 M NaOH solution at different irradiation times. b) Normalized fluorescence intensity per unit surface area with different photocatalysts. The inset in (a) shows the time dependences of the fluorescence intensity at 426 nm, where squares are clean cuboids and triangles are F-cuboids, respectively.

3. Conclusions

Uniform, well-defined, anatase TiO_2 nanocuboids enclosed by active {100} and {001} facets over a wide size range (60–830 nm in length) with controllable aspect ratios were solvothermally synthesized through hydrolysis of TTIP using HAc as the solvent and [bmim][BF_4] as the capping agent. The size and aspect ratio of the anatase TiO_2 nanocuboids can be readily adjusted by changing the composition parameters including the contents of water (x), [bmim][BF_4] (y) and HAc (z) in the quaternary solution system. While both the increase in the

© 2011 WILEY-VCH Verlag GmbH & Co. KGaA, Weinheim

content of water and the decrease in the HAc content brought about the decrease in the size of the nanocuboids owing to an accelerated hydrolysis-condensation process, the increase in both the water content and the HAc content resulted in the decrease in the aspect ratio of the nanociuboids or the percentage of the {100} facets. It has been revealed that the ionic liquid [bmim][BF_4] played an important role in stabilizing both the {100} and {001} facets of the anatase TiO_2 nanocuboids. On the one hand, [bmim][BF_4] acted as an environmentally friendly and easy-to-operate fluoride source to release F^- ions for stabilizing the {001} facets; on the other hand, the $[bmim]^+$ ions acted as effective capping ions to preferentially stabilize the {100} facets. The obtained near-monodisperse anatase TiO_2 nanocuboids exhibited interesting self-assembly behavior during deposition, indicating their potential applications as unique building blocks for constructing hierarchically ordered assemblies or colloidal crystals with novel properties. These single-crystalline anatase nanocuboids showed extremely high crystalline phase stability, retaining the pure phase of anatase as well as the morphology even after being calcined at 900 °C, which would enable their potential long-term applications in high-temperature environments. Furthermore, the anatase TiO_2 nanocuboids exhibited considerably enhanced photocatalytic activity owing the exposed active {100} and {001} facets. These anatase TiO_2 nanocuboids almost exclusively enclosed by the {100} and {001} facets may be employed as an ideal model system for fully evaluating the order of facet reactivity of anatase crystals for different photocatalytic reactions. This synthetic approach is very simple and reproducible, which may be extendable to the controlled synthesis of other functional oxide crystals with well-defined morphologies and tunable sizes and percentages of exposed facets.

4. Experimental Section

Materials: 1-Butyl-3-methylimidazolium tetrafluoroborate ([bmim][BF_4]) and 1-*n*-butyl-3-methylimidazolium chloride ([bmim]Cl) were obtained from Alfa Aesar, and sodium fluoroborate (Na[BF_4]) was purchased from Sinopharm Chemical Reagent Co. Titanium tetraisopropoxide (TTIP) was obtained from Acros, and acetic acid (HAc) and hydrofluoric acid (40%) were purchased from Beijing Chemical Works. Degussa P25 was obtained from Beijing Entrepreneur Science & Trading Co. All chemicals were used as received without further purification. The water used was deionized.

Synthesis of Anatase TiO_2 Nanocuboids: Anatase TiO_2 nanocuboids with varied sizes and aspect ratios were synthesized in a quaternary solution system consisting of TTIP, deionized water, [bmim][BF_4], and HAc, with molar ratios of TTIP/H_2O/[bmim][BF_4]/HAc at 1:*x*:*y*:*z*. In a typical synthesis, 200 µL of [bmim][BF_4], 20 µL of water, and 8 mL of HAc were mixed in a dried Teflon autoclave with a capacity of 20 mL. Then, 200 µL of TTIP was added, giving a mixture with molar ratios of TTIP/H_2O/[bmim][BF_4]/HAc at 1:1.66:2:210, which was then kept at 200 °C for 24 h. After being cooled to room temperature, the resultant white powder was separated by centrifugation and washed with ethanol for several times, dried at 60 °C overnight. In the synthesis, the contents of water (*x*), [bmim][BF_4] (*y*) and HAc (*z*) were systematically changed to obtain anatase TiO_2 nanocuboids with different sizes and aspect ratios. For investigation of the effect of the ionic liquid [bmim][BF_4], it was replaced by [bmim]Cl, Na[BF_4], or a mixture of [bmim]Cl and HF in certain cases.

Characterization: The obtained products were characterized by scanning electron microscopy (SEM, Hitachi S4800, 15 kV), transmission electron microscopy (TEM, JEOL JEM 200CX, 160 kV), high-resolution TEM (HRTEM, FEI Tecnai F30, 300 kV), powder X-ray diffraction (XRD, Rigaku Dmax-2000, Cu KR), X-ray photoelectron spectroscopy (XPS, Kratos Axis Ultra spectrometer with monochromatized Al Kα radiation), and Fourier transform infrared spectroscopy (FTIR, Nicolet Magna-IR 750). The Brunauer–Emmett–Teller (BET) specific surface area was measured using a Micromeritics ASAP 2010 instrument and the fluorescence spectra were recorded on a Hitachi F-4500 FL spectrophotometer.

Photocatalysis Measurement: The surface fluorine and other residual organic compounds were removed to obtain fluorine-free, clean anatase nanocuboids through a heat treatment process at 800 °C for 3 h. For the photocatalysis measurement, 25 mg of photocatalysts, such as fluorine-free anatase nanocuboids (clean cuboids), fluorine-capped anatase nanocuboids (F-cuboids), fluorine-free anatase sheets (clean sheets), and P25, were suspended in 100 mL of aqueous solution containing 0.01 M NaOH and 3.0 mM terephthalic acid and stirred in the dark for 30 min. Then, the suspension was exposed to UV irradiation using an 8 W U-type UV lamp with a maximum emission at 254 nm. 5.0 mL of solution was taken out every 20 min, and the TiO_2 was separated from the solution by centrifugation. The remaining clear liquid was used for fluorescence spectrum measurements. During the photoreactions, no oxygen was bubbled into suspension.

Supporting Information

Supporting Information is available from the Wiley Online Library or from the author.

Acknowledgements

This work was supported by NSFC (21073005, 20873002, and 50821061) and MOST (2007CB936201).

Received: March 21, 2011
Revised: May 8, 2011
Published online: July 25, 2011

[1] Z.-Y. Jiang, Q. Kuang, Z.-X. Xie, L.-S. Zheng, *Adv. Funct. Mater.* **2010**, *20*, 3634.
[2] N. Tian, Z. Y. Zhou, S. G. Sun, Y. Ding, Z. L. Wang, *Science* **2007**, *316*, 732.
[3] H. G. Yang, C. H. Sun, S. Z. Qiao, J. Zou, G. Liu, S. C. Smith, H. M. Cheng, G. Q. Lu, *Nature* **2008**, *453*, 638.
[4] X. Xie, Y. Li, Z. Q. Liu, M. Haruta, W. Shen, *Nature* **2009**, *458*, 746.
[5] a) X. Chen, S. S. Mao, *Chem. Rev.* **2007**, *107*, 2891; b) A. Fujishima, X. Zhang, D. A. Tryk, *Surf. Sci. Rep.* **2008**, *63*, 515; c) M. Grätzel, *Nature* **2001**, *414*, 338; d) D. Deng, M. G. Kim, J. Y. Lee, J. Cho, *Energy Environ. Sci.* **2009**, *2*, 818; e) P. Roy, S. Berger, P. Schmuki, *Angew. Chem. Int. Ed.* **2011**, *50*, 2904.
[6] a) S. Liu, J. Yu, M. Jaroniec, *J. Am. Chem. Soc.* **2010**, *132*, 11914; b) J. S. Chen, Y. L. Tan, C. M. Li, Y. L. Cheah, D. Luan, S. Madhavi, F. Y. C. Boey, L. A. Archer, X. W. Lou, *J. Am. Chem. Soc.* **2010**, *132*, 6124; c) W. Yang, J. Li, Y. Wang, F. Zhu, W. Shi, F. Wan, D. Xu, *Chem. Commun.* **2011**, *47*, 1809.
[7] U. Diebold, *Surf. Sci. Rep.* **2003**, *48*, 53.
[8] a) A. Beltran, J. R. Sambrano, M. Calatayud, F. R. Sensato, J. Andrés, *Surf. Sci.* **2001**, *490*, 116; b) M. Calatayud, C. Minot, *Surf. Sci.* **2004**, *552*, 169.
[9] M. Lazzeri, A. Vittadini, A. Selloni, *Phys. Rev. B.* **2001**, *63*, 155409.
[10] B. Wu, C. Guo, N. Zheng, Z. Xie, G.. D. Stucky, *J. Am. Chem. Soc.* **2008**, *130*, 17563.
[11] a) Y. Dai, C. M. Cobley, J. Zeng, Y. Sun, Y. Xia, *Nano Lett.* **2009**, *9*, 2455; b) D. Zhang, G. Li, H. Wang, K. M. Chan, J. C. Yu, *Cryst. Growth Des.* **2010**, *10*, 1130.

© 2011 WILEY-VCH Verlag GmbH & Co. KGaA, Weinheim

[12] a) H. G. Yang, G. Liu, S. Z. Qiao, C. H. Sun, Y. G. Jin, S. C. Smith, H. M. Cheng, G. Q. Lu, *J. Am. Chem. Soc* **2009**, *131*, 4078; b) X. Han, Q. Kuang, M. Jin, Z. Xie, L. Zheng, *J. Am. Chem. Soc.* **2009**, *131*, 3152.

[13] a) D. Zhang, G. Li, X. Yang, J. C. Yu, *Chem. Commun.* **2009**, 4381; b) G. Liu, C. Sun, H. G. Yang, S. C. Smith, L. Wang, G. Q. Lu, H. M. Cheng, *Chem. Commun.* **2010**, *46*, 755; c) C. H. Sun, X. H. Yang, J. S. Chen, Z. Li, X. W. Lou, C. Li, S. C. Smith, G. Q. Lu, H. G. Yang, *Chem. Commun.* **2010**, *46*, 6129; d) J. Yu, J. Fan, K. Lv, *Nanoscale* **2010**, *2*, 2144; e) J. Zhu, S. Wang, Z. Bian, S. Xie, C. Cai, J. Wang, H. Yang, H. Li, *CrystEngComm* **2010**, *12*, 2219.

[14] a) Z. Zheng, B. Huang, X. Qin, X. Zhang, Y. Dai, M. Jiang, P. Wang, M. H. Whangbo, *Chem. Eur. J.* **2009**, *15*, 12576; b) X. Wang, B. Huang, Z. Wang, X. Qin, X. Zhang, Y. Dai, M.-H. Whangbo, *Chem. Eur. J.* **2010**, *16*, 7106; c) H. Zhang, Y. Han, X. Liu, P. Liu, H. Yu, S. Zhang, X. Yao, H. Zhao, *Chem. Commun.* **2010**, *46*, 8395; d) X. Y. Ma, Z. G. Chen, S. B. Hartono, H. B. Jiang, J. Zou, S. Z. Qiao, H. G. Yang, *Chem. Commun.* **2010**, *46*, 6608; e) W. Q. Fang, J. Z. Zhou, J. Liu, Z. G. Chen, C. Yang, C. H. Sun, G. R. Qian, J. Zou, S. Z. Qiao, H. G. Yang, *Chem. Eur. J.* **2011**, *17*, 1423; f) M. Liu, L. Piao, W. Lu, S. Ju, L. Zhao, C. Zhou, H. Lia, W. Wang, *Nanoscale* **2010**, *2*, 1115; g) J. Yu, Q. Xiang, J. Rana, S. Mann, *CrystEngComm* **2010**, *12*, 872; h) J. S. Chen, C. Chen, J. Liu, R. Xu, S. Z. Qiao, X. W. Lou, *Chem. Commun.* **2011**, *47*, 2631.

[15] P. Wen, H. Itoh, W. Tang, Q. Feng, *Langmuir.* **2007**, *23*, 11782.

[16] C.-T. Dinh, T.-D. Nguyen, F. Kleitz, T.-O. Do, *ACS Nano* **2009**, *3*, 3737.

[17] J. Li, D. Xu, *Chem. Commun.* **2010**, *46*, 2301.

[18] J. Pan, G. Liu, G. Q. Lu, H.-M. Cheng, *Angew. Chem. Int. Ed.* **2011**, *50*, 2133.

[19] C. Z. Wen, J. Z. Zhou, H. B. Jiang, Q. H. Hu, S. Z. Qiao, H. G. Yang, *Chem. Commun.* **2011**, *47*, 4400.

[20] a) Z. Ma, J. Yu, S. Dai, *Adv. Mater.* **2010**, *22*, 261; b) J. Dupont, J. D. Scholten, *Chem. Soc. Rev.* **2010**, *39*, 1780.

[21] a) Y. Qin, Y. Song, N. Sun, N. Zhao, M. Li, L. Qi, *Chem. Mater.* **2008**, *20*, 3965; b) Y. Qin, Y. Song, T. Huang, L. Qi, *Chem. Commun.* **2011**, *47*, 2985.

[22] K. Ding, Z. Miao, Z. Liu, Z. Zhang, B. Han, G. An, S. Miao, Y. Xie, *J. Am. Chem. Soc.* **2007**, *129*, 6362.

[23] J. Ye, W. Liu, J. Cai, S. Chen, X. Zhao, H. Zhou, L. Qi, *J. Am. Chem. Soc.* **2011**, *133*, 933.

[24] a) P. D. Cozzoli, A. Kornowski, H. Weller, *J. Am. Chem. Soc.* **2003**, *125*, 14539; b) X.-L. Li, Q. Peng, J.-X. Yi, X. Wang, Y. Li, *Chem. Eur. J.* **2006**, *12*, 2383.

[25] Y. Wang, H. Zhang, Y. Han, P. Liu, X. Yao, H. Zhao, *Chem. Commun.* **2011**, *47*, 2829.

[26] a) K. J. M. Bishop, C. E. Wilmer, S. Soh, B. A. Grzybowski, *Small* **2009**, *5*, 1600; b) U. Agarwal, F. A. Escobedo, *Nat. Mater.* **2011**, *10*, 230; c) Z. Zhu, H. Meng, W. Liu, X. Liu, J. Gong, X. Qiu, L. Jiang, D. Wang, Z. Tang, *Angew. Chem. Int. Ed.* **2011**, *50*, 1593.

[27] X. W. Lou, H. C. Zeng, *J. Am. Chem. Soc.* **2003**, *125*, 2697.

[28] a) K. L. Ding, Z. J. Miao, B. J. Hu, G. M. An, Z. Y. Sun, B. X. Han, Z. M. Liu, *Langmuir* **2010**, *26*, 5129; b) K. L. Ding, Z. J. Miao, B. J. Hu, G. M. An, Z. Y. Sun, B. X. Han, Z. M. Liu, *Langmuir* **2010**, *26*, 10294.

[29] J. Lian, X. Duan, J. Ma, P. Peng, T. Kim, W. Zheng, *ACS Nano* **2009**, *3*, 3749.

[30] a) D. S. Jacob, L. Bitton, J. Grinblat, I. Felner, Y. Koltypin, A. Gedanken, *Chem. Mater.* **2006**, *18*, 3162; b) Z. J. Miao, Z. M. Liu, K. L. Ding, B. X. Han, S. D. Miao, G. M. An, *Nanotechnology* **2007**, *18*, 125605.

[31] C. Li, L. Gu, S. Tsukimoto, P. A. van Aken, J. Maier, *Adv. Mater.* **2010**, *22*, 3650.

[32] W. Zheng, X. Liu, Z. Yan, L. Zhu, *ACS Nano* **2009**, *3*, 115.

[33] D. A. H. Hanaor, C. C. Sorrell, *J. Mater. Sci.* **2011**, *46*, 855.

[34] a) N. T. Nolan, M. K. Seery, S. C. Pillai, *J. Phys. Chem. C* **2009**, *113*, 16151; b) C. Kang, L. Jing, T. Guo, H. Cui, J. Zhou, H. Fu, *J. Phys. Chem. C* **2009**, *113*, 1006.

[35] a) J. Zhang, M. Li, Z. Feng, J. Chen, C. Li, *J. Phys. Chem. B* **2006**, *110*, 927; b) J. Zhang, Q. Xu, M. Li, Z. Feng, C. Li, *J. Phys. Chem. C* **2009**, *113*, 1698.

[36] T. Hirakawa, Y. Nosaka, *Langmuir.* **2002**, *18*, 3247.

© 2011 WILEY-VCH Verlag GmbH & Co. KGaA, Weinheim